A snow cover climatology for the Pyrenees from MODIS snow products

S. Gascoin[1]**, O. Hagolle**[1]**, M. Huc**[1]**, L. Jarlan**[1]**, J.-F. Dejoux**[1]**, C. Szczypta**[1]**, R. Marti**[1,2]**, and R. Sánchez**[3]

[1]Centre d'Etudes Spatiales de la Biosphère (CESBIO), UPS/CNRS/IRD/CNES, Toulouse, France
[2]Géographie de l'Environnement (GEODE), UT2J/CNRS, Toulouse, France
[3]Confederación Hidrográfica del Ebro, Zaragoza, Spain

Correspondence to: S. Gascoin (simon.gascoin@cesbio.cnes.fr)

Abstract

The seasonal snow in the Pyrenees is critical for hydropower production, crop irrigation and tourism in France, Spain and Andorra. Complementary to in situ observations, satellite remote sensing is useful to monitor the effect of climate on the snow dynamics. The MODIS daily snow products (Terra/MOD10A1 and Aqua/MYD10A1) are widely used to generate snow cover climatologies, yet it is preferable to assess their accuracies prior to their use. Here, we use both in situ snow observations and remote sensing data to evaluate the MODIS snow products in the Pyrenees. First, we compare the MODIS products to in situ snow depth (SD) and snow water equivalent (SWE) measurements. We estimate the values of the SWE and SD best detection thresholds to 40 mm water equivalent (we) and 150 mm respectively, for both MOD10A1 and MYD10A1. Kappa coefficients are within 0.74 and 0.92 depending on the product and the variable. Then, a set of Landsat images is used to validate MOD10A1 and MYD10A1 for 157 dates between 2002 and 2010. The resulting accuracies are 97 % ($\kappa = 0.85$) for MOD10A1 and 96 % ($\kappa = 0.81$) for MYD10A1, which indicates a good agreement between both datasets. The effect of vegetation on the results is analyzed by filtering the forested areas using a land cover map. As expected, the accuracies decreases over the forests but the agreement remains acceptable (MOD10A1: 96 %, $\kappa = 0.77$; MYD10A1: 95 %, $\kappa = 0.67$). We conclude that MODIS snow products have a sufficient accuracy for hydroclimate studies at the scale of the Pyrenees range. Using a gapfilling algorithm we generate a consistent snow cover climatology, which allows us to compute the mean monthly snow cover duration per elevation band and aspect classes. There is snow on the ground at least 50% of the time above 1600 m between December and April. We finally analyze the snow patterns for the atypical winter 2011–2012. Snow cover duration anomalies reveal a deficient snowpack on the Spanish side of the Pyrenees, which seems to have caused a drop in the national hydropower production.

1 Introduction

The Pyrenees mountain range is located in southwest Europe at the northern edge of the Iberian peninsula (43° N, maximum elevation 3404 m a.s.l., Fig. 1). Because of the large amount of precipitation it receives, the Pyrenees range is the water tower for a region cov-
³⁰ ering northern Spain, Andorra and south France. The headwaters of three major rivers in southwest Europe, namely the Ebro, the Garonne and the Adour rivers are located in the Pyrenees mountains. These rivers and their tributaries provide critical water resources for various economic activities, including hydropower generation and crop production in the irrigated lowlands.

³⁵ As most of the winter precipitation falls as snow in the Pyrenees, the snow melt is an important contributor to the river flow and shapes the hydrographs of the Pyrenean rivers (Lopez-Moreno and Garcia-Ruiz, 2004; Bejarano et al., 2010). Spring snowmelt is extensively used in downstream areas for crop irrigation during the growing season. Snowmelt is also stored in the many reservoirs located on the Pyrenean foothills. The main functions of
⁴⁰ these reservoirs are to supply runoff for irrigation in summer and to produce hydropower. For example in the Ebro basin there are 299 operating dams, according to the governmental inventory (Ministerio de Agricultura, Alimentación y Medio Ambiente, 2011). The unofficial inventory from the Spanish association of dams and reservoirs (Sociedad Española de Presas y Embalses, 2008) indicates that at least one fourth of the dams in the Ebro basin are
⁴⁵ used for irrigation and two thirds for hydropower generation (other uses include river regulation, aquafarming, water supply to urban and industrial areas, etc.). In addition, many hydroelectric plants in the Pyrenees also work without the use of a dam (run-of-the-river hydroelectricity). As a result, 33 % of the hydroelectricity power plants in Spain are located in the Ebro basin, most of them being connected to the Pyrenean rivers (Fig. 2). The potential
⁵⁰ hydropower of the Ebro basin represents 19.5 % of the total potential hydropower in Spain (Ministerio de Agricultura, Alimentación y Medio Ambiente, 2011). In France, the Pyrenean rivers are also highly exploited for irrigation and hydroelectricity (Fig. 2). The Garonne river is known as the only large watershed in France where a structural imbalance between wa-

3

ter resources, the needs of different users and aquatic environments is officially recognized
55 (Dupeyrat et al., 2008). The rising pressure on the water resources in the Ebro basin is also
an important concern (Milano et al., 2013).

Apart from these hydrological services, the snow cover is also critical for the tourism
sector in the Pyrenees. In particular ski resorts are an important source of income and local
employment (Rived et al., 2013).

60 Given the importance of the snow cover in the Pyrenees, it is necessary to monitor its evo-
lution. The snow depth is recorded daily at 19 stations at least across the whole Pyrenees
mountain range. Some stations were already installed in the 1980's but most of the data are
available since the 2000's. Yet, these ground measurements are essential but insufficient to
describe the snow cover dynamics in the various topographic and climatic contexts of the
65 Pyrenees mountain range. On the other hand, remote sensing data are spatially consistent
and therefore can be very useful to complement in situ measurements.

Since the early 1980's, it has been shown that space-borne sensors operating in the visi-
ble and near-infrared region of the electromagnetic spectrum are very effective to map snow
cover (Bowley et al., 1981; Dozier and Marks, 1987; Baumgartner et al., 1987). As of today,
70 only low to mid-resolution sensors such as AVHRR, PROBA-V or MODIS allow global ob-
servations of the snow cover at daily time step (without cloud obstruction) with a spatial res-
olution of 1 km to 250 m. Higher resolution snow cover maps (30 m) are typically extracted
from the Landsat program images, but they provide data at a lower frequency (16 days),
which is generally inappropriate to monitor the snow cover as large snow area variations
75 can occur within a few days during the melt season (Rango, 1993; Gómez-Landesa and
Rango, 2002).

A suite of snow products were derived from Aqua and Terra MODIS data and released
in 2000 (Hall et al., 2002). The MODIS snow products are now widely used for hydro-
climate applications in snow dominated regions. These products were generated using
80 the SNOMAP algorithm, which primarily relies on the Normalized Difference Snow Index
(NDSI). The Normalized Difference Vegetation Index (NDVI) is also used to improve snow
detection in forested areas (Klein et al., 1998). There are differences between Aqua and

4

Terra products as Aqua MODIS band 6 detectors are not functioning, while band 6 is used for the Terra product to compute the NDVI (Hall and Riggs, 2007). As a consequence the NDVI test for forested areas is not activated for Aqua products. The successive versions of the MODIS snow products were compared with snow maps obtained from other sources at similar or lower resolution (i.e. relative validation, Hall et al., 2002; Klein and Barnett, 2003; Maurer et al., 2003; Simic et al., 2004; Rittger et al., 2013) and validated using ground snow measurements (i.e. absolute validation) (Klein and Barnett, 2003; Maurer et al., 2003; Simic et al., 2004; Ault et al., 2006; Parajka and Blöschl, 2006; Arsenault et al., 2014). Most of these studies were done using the Terra MODIS daily snow product (MOD10A1). More comprehensive reviews can be found in Hall and Riggs (2007) and Parajka et al. (2012). Despite the variety of methods used among these studies, the results led to the same conclusion that Terra MODIS snow cover products have a higher overall accuracy than snow maps derived from VEGETATION or AVHRR. The typical absolute accuracy of MOD10A1 is 93 % but depends on the land cover (Hall and Riggs, 2007; Arsenault et al., 2014). The accuracy is lower in forested areas (Simic et al., 2004; Parajka et al., 2012). Other important sources of misdetection are cloud/snow confusion (Rittger et al., 2013), the variation of the sensor viewing angle and the reprojection from the original swath data to the sinusoid grid (Arsenault et al., 2014). The accuracy of Aqua snow product is similar although less documented. A comparison with Terra snow maps indicated a lower accuracy at least in forested areas as expected (Hall and Riggs, 2007).

Alternative snow cover detection algorithms were developed for MODIS reflectance data, which showed better accuracies (Sirguey et al., 2008; Rittger et al., 2013). However these codes are not operational globally and imply the processing of large amount of data to get a snow map, which restrict the number of potential users. In contrast, MODIS snow products are available at the global scale through Internet usually with a short delay of eight days.

The comparison with ground data is a robust and precise method to validate satellite snow maps. However, a limitation is that the spatial representativeness of each measurement is generally unknown. It can be assumed that a ground observation is valid for the whole pixel above a certain snow depth threshold (Maurer et al., 2003). The other type of

validation is performed using Landsat-derived snow maps as a reference, since Landsat high-resolution data allow an accurate detection of snow even in mountains (Salomonson and Appel, 2004; Hall and Riggs, 2007). The advantage of this method is that there is no issue on the spatial representativeness of the reference data. Moreover, it allows an evaluation of MODIS snow maps in regions where the in situ station network for snow monitoring is insufficient. This technique was initially used to assess the SNOMAP algorithm (Hall et al., 1995, 2002; Klein et al., 1998). The comparison was limited to one or a few Landsat scenes with low or null cloud coverage. The small numbers of scenes allowed a manual removal of clouds. Since 2009, the Landsat archive is freely accessible, which enables to generate many snow maps over a large area for various periods of the year. This allows the assessment of MODIS snow products for varying snow conditions (e.g. fresh snow in winter, ripe snow in spring). Recently, Rittger et al. (2013) have taken advantage of this exceptional archive to validate the MODIS snow products. They found large errors during the snowmelt period and in forest areas, and conclude that MODIS snow products still require to be used with caution.

The main objectives of this study are twofold:

  – First, we aim to evaluate the value of the MOD10A1 snow product to generate a daily snow cover climatology in the Pyrenees for the period 2000–2013.

  – Second, we use this new dataset to characterize the variability of the snow cover in the Pyrenees.

The first objective is a necessary step even though many studies have already assessed the MODIS snow products accuracy in other mountainous regions. Indeed, continuing validation is important to make the information reliable, since the combination of topography, land cover and climate varies from one region to another (Rittger et al., 2013). In our case, the Pyrenees present a large physiographic variability in a rather small area and is under the influences of both Mediterranean and north-Atlantic climates. Moreover, this assessment is important because the MODIS snow products are getting more and more attention from the regional agencies in charge of the water and tourism management in the Pyre-

6

140 nees (Parra et al., 2006). In particular, an important question for the water practitioners is the effective snow detection threshold, i.e. the value of the snow water equivalent or snow depth for which a pixel is statistically marked as snow covered in a MODIS product.

We used both in situ and remote sensing data to assess both Aqua and Terra MODIS daily snow cover binary products (snow/no snow) in the Pyrenees. For the first time, we as-
145 sembled a French–Spanish dataset of continuous snow measurements from the Ebro basin agency in Spain and Météo-France. This dataset was used to validate the MODIS snow products and to determine the optimal snow detection threshold. Then, Landsat scenes over the Pyrenees corresponding to 157 dates between 2002 and 2010 were processed to generate an independent snow cover product. We did not focus on the discrepancies
150 between the MODIS products and the Landsat or station data on specific dates or regions. We rather aimed at characterizing the range of uncertainties at the scale of the Pyrenees mountain range and across the snow season.

For the second objective, we implemented a gap-filling algorithm based on previous studies to generate a gap-free snow cover climatology from February 2000 to July 2013. This
155 allows us to characterize the variability of the snow cover duration at the scale of the whole Pyrenees and its relationship with the topography. We show an application of this climatology to characterize the anomalous snow cover patterns during the 2011–2012 winter, which was particularly dry in the southern Pyrenees (San Ambrosio et al., 2013).

2 Data and methods

160 ### 2.1 Data

2.1.1 In situ data

We assembled two important datasets of in situ snowpack monitoring in the Pyrenees (Table 1). Météo-France provided the snow depth observations at 8 stations in the French Pyrenees from January 2000 to December 2010. The snow depth was recorded daily at

7

165 06:00 UTC with a 1 cm resolution. The Ebro basin agency (Confederación Hidrográfica del Ebro) provided the snow depth and snow water equivalent data from 11 telenivometers in the Spanish Pyrenees managed as part of the ERHIN program (Evaluación de los Recursos Hídricos procedentes de la Innivación, study of winter water resources) (Parra et al., 2006). Each telenivometer is equipped with an acoustic snow gauge and a cosmic ray

170 detector for snow water equivalent sensing (Paquet and Laval, 2006). The snow season is generally shorter at Météo-France stations (e.g. Aulus-Les-Bains, Bagneres-de-Luchon, St-Lary-Soul) because they are located at lower elevation than the telenivometers (Table 1).

2.1.2 Landsat

We used the data acquired by Landsat 5 Thematic Mapper (TM) and Landsat-7 Enhanced

175 Thematic Mapper Plus (ETM+). The data were collected from the United States Geological Survey (USGS) and the European Space Agency (ESA). The Landsat scenes spanning the Pyrenees are numbered 200-030 to 197-030 in the Worldwide Reference System 2 (eastward). There are 157 dates in our dataset distributed between January 2002 and December 2010 for which at least one of these Landsat scenes is available.

180 ### 2.1.3 MODIS snow products

MOD10A1 (Terra) and MYD10A1 (Aqua) snow products version 5 were downloaded from the National Snow and Ice Data Center (Hall et al., 2006, 2007) for the period 1 September 2000 to 2 July 2013. This corresponds to 4688 days among which 4625 days are available for MOD10A1 (98.7 %) and 3996 dates for MYD10A1 (85.4 %) since Aqua was

185 launched in May 2002 and operational in July 2002. From this archive 157 MOD10A1 were available on the same day as the Landsat dataset for MOD10A1 and 139 dates for MYD10A1.

We also downloaded the MOD10A2 product, which provides the maximum snow extent from MOD10A1 over a compositing period of 8 days on the same grid.

8

2.1.4 Land cover

We used the Corine land cover 2000 raster data version 15 that covers both France and Spain. It is considered as a reference data for land cover mapping at the Europe scale (Bossard et al., 2000). The Corine land cover was used to produce a map of forested areas by aggregation of the broad-leaved forest, coniferous forest, and mixed forest classes (63 % of the study area).

2.2 Methods

2.2.1 In situ data processing

Some snow depth or snow water equivalent values from the telenivometer dataset were negative in summer, probably because of a drift in the sensors calibration factors. These negative values were set to zero. Otherwise the data were not filtered or corrected.

2.2.2 Landsat processing

The processing of a large number of Landsat images is only feasible with an automatic cloud detection algorithm because the cloud mask is not provided with the Landsat data. Here we applied a cloud detection algorithm developed for high-resolution multispectral images from Landsat, Venμs and Sentinel-2 (Hagolle et al., 2010).

The Landsat data were processed as follows:

- Orthorectification: Landsat data available from USGS are already orthorectified. Hence, ESA data were orthorectified using USGS data as a reference following the orthorectification methodology of the Centre National d'Etudes Spatiales (Baillarin et al., 2004). All images were projected to Lambert-93. The superposition errors were 0.2 to 0.8 pixels for USGS data and 0.3 to 0.9 for ESA data depending on cloud coverage.

- Radiometric calibration for both datasets was made following (Chander et al., 2009). The radiometric accuracy is not critical for this application.

- **–** The scenes were assembled and resampled to a 240 m resolution.

215 **–** The cloud mask and cloud shadows mask were retrieved based on the detection of abrupt changes in the reflectance time series for every pixel (multi-temporal algorithm, Hagolle et al., 2010).

- **–** An external mask of water bodies was applied (SRTM water body data)

- **–** The snow cover was detected based on the NDSI and the reflectance in the green 220 and SWIR channels (Dozier, 1989). The NDSI was defined as:

$$NDSI = \frac{\rho_{green} - \rho_{SWIR}}{\rho_{green} + \rho_{SWIR}} \tag{1}$$

where ρ_{green} (resp. ρ_{SWIR}) is the top of atmosphere reflectance in Landsat green channel (resp. shortwave infrared at 1.6 µm). A pixel is flagged as snow if the three following 225 conditions are fulfilled:

1. $NDSI > 0.4$,
2. $\rho_{red} > 0.12$
3. $\rho_{SWIR} < 0.16$.

These criteria were applied on reflectance corrected for a first-order slope effect (co-230 sine correction Meyer et al., 1993). If a group of adjacent pixels was detected as snow but entirely surrounded by cloud-covered pixels, then these pixels were flagged as cloud, otherwise thick cold clouds may be detected as snow. The mask generated with these criteria was dilated with a circular radius of three pixels to improve the detection on the snow region boundaries, which have a smaller snow thickness and generally 235 do not fulfill all the three previous conditions. These steps and the red and SWIR reflectance thresholds were adjusted from the original formulation (Dozier, 1989) based on a visual inspection of the full resolution images over the study area.

10

2.2.3 MODIS snow products processing

We extracted the "Snow Cover Daily Tile" field from MOD10A1 and MYD10A1, which in-
cludes the snow/no snow and cloud masks. Our zone intersects the MODIS sinusoid grid
tiles h17v04 and h18v04. The grids were assembled and reprojected with the nearest-
neighbor method in Lambert-93 over a region of interest covering the Pyrenees using the
MODIS reprojection tool (extent given in Fig. 1). The different classes in the original prod-
uct were merged in three classes: no-snow (no snow or lake), snow (snow or lake ice),
no-data (clouds, missing data, no decision, saturated detector). The MODIS snow masks
corresponding to the Landsat dates were also resampled to a 240 m resolution in order to
match our Landsat snow mask spatial resolution.

In a second phase of this work we implemented a gap-filling algorithm to interpolate
virtually all the missing values from 1 September 2000 to 1 July 2013. The algorithm was
derived from Parajka and Blöschl (2008) and works in four sequential steps:

1. Aqua/Terra combination: for every pixel if no-data was found in MOD10A1 then the
   value from MYD10A1 was taken. Otherwise, the value in MOD10A1 was kept. The
   priority was given to MOD10A1 because we found that MYD10A1 is less accurate
   (see Sect. 3).

2. Adjacent spatial deduction: each no-data pixel was reclassified as snow (no-snow) if
   at least five of the eight adjacent pixels were classified as snow (no-snow).

3. Adjacent temporal deduction: a no-data pixel was reclassified as snow (no-snow) if the
   same pixel was classified as snow (no-snow) in both the preceding and the antecedent
   grid. The preceding and antecedent grids were searched within a sliding temporal
   window, whose size was incremented if there was still a no-data value. This means
   that if a pixel was marked as no-data in grid $n + 1$ and/or in grid $n - 1$ (sliding window
   of 2 days), then the algorithm started again with a sliding window of 3 days (i.e. the
   test was done with grids $n + 1$ and $n - 2$, or grids $n + 2$ and grid $n - 1$). For this study
   we allowed the window size to be incremented up to 9 days in order to fill a long gap

²⁶⁵ from 20 March 2002 to 28 March 2002 included. The longest data gap lasted 17 days in summer 2001 due to a power supply failure of the MODIS instrument on board Terra (15 June 2001 to 2 July 2001). This gap was not filled because this period is not critical for snow cover monitoring.

4. The sparse remaining no-data pixels were reclassified using a classification tree ²⁷⁰ (Breiman et al., 1984, Matlab Statistics Toolbox). For each date, the snow and no-snow pixels were used to fit a classification tree on four predicting variables derived from the geographic position and the topography. The variables were: pixel elevation, aspect, easting and northing (i.e. x and y coordinates in Lambert-93). The tree was used to predict the class of the no-data pixels for this date.

²⁷⁵ The gapfilled pixels were flagged in the final product to maintain record of the original data.

2.2.4 Comparison

We computed the confusion matrices between the MODIS product snow/no snow classification and both reference datasets (i.e. in situ data or Landsat data), which were considered ²⁸⁰ as the truth. Based on these results we computed the overall accuracy, precision and the kappa coefficient (Cohen, 1960, noted κ). The overall accuracy (AC) is the proportion of the total number of predictions that were correct (i.e. snow or no snow). The precision (P) is the proportion of the predicted snow presences that were correct. In the analysis, we mainly used the kappa coefficient because this statistic incorporates both information on ²⁸⁵ agreement and disagreement between the MODIS products and the validation data (Klein and Barnett, 2003). For in situ data, the comparison was performed both for snow water equivalent (SWE) and snow depth (SD) measurements.

1. In situ data: the MODIS product snow presence/absence was extracted at each station. For each date, a pixel was considered to be correctly classified as snow if the ²⁹⁰ snow depth value on the same day (or the SWE value) is higher than a threshold value noted SD_0 (or SWE_0). We tested 40 logarithmically spaced values between 0

12

and 8 m for SD_0 and 0 and 3 m.w.e. for SWE_0. The same method was applied to the SWE data from the telenivometers, the SD data from the telenivometers alone and the SD data from all stations.

²⁹⁵ 2. Landsat data: every pair of MODIS and Landsat snow masks obtained on the same day was compared on a pixel-basis. The comparison was made only for the pixels which were not masked by the union of MODIS and Landsat cloud masks (i.e. where snow or no snow detection was possible for both datasets). For MOD10A1, a total of 14.7×10^6 pixels were compared with the Landsat snow masks, among which 13.4 % ³⁰⁰ were classified as snow in the Landsat data.

The gapfilled product was also evaluated by comparison with the in situ data. The comparison with Landsat was not performed because most of the no-data pixels are due to cloud cover, which also obstructed the Landsat image on the same day. However, we compared our gapfilled product with the 8 day composite product MOD10A2, which is often used ³⁰⁵ in hydrometeorological studies.

3 Results

3.1 In situ data vs. MODIS products

A first visual inspection of the time series suggests that there is a good agreement between in situ observations and the MODIS product, as shown here in the case of Ordiceto station ³¹⁰ only (Fig. 3).

From these data an optimal SWE detection threshold is found between 20 and 60 mm w.e. (top row in Fig. 4). For SD, the range of optimal values is narrower between 100 and 120 mm (middle and bottom rows in Fig. 4). The optimum is nearly identical for MYD10A1 but the agreement is a bit lower than for MOD10A1 as indicated by the kappa curve. In what fol-³¹⁵ lows, we have set $SWE_0 = 40$ mm w.e. and $SD_0 = 150$ mm (Table 2). The resulting confusion matrices (Table 2) and statistical measures (Table 3) further indicate that an excellent

13

agreement is found between the SWE data and MOD10A1 ($\kappa = 0.95$), but the agreement decreases if MYD10A1 is considered. Another result is that the classification accuracy is higher with the SWE variable than with SD variable for the same stations (Table 2). The

320 agreement between MODIS and in situ data significantly decreases when considering SD for all available stations (Table 3). In any case, however, the agreement remains acceptable since the lowest kappa is 0.74.

The seasonal differences in the detection threshold were further analyzed based on the SD data from the telenivometers and MOD10A1 (Fig. 5). The results show that there is a

325 trend in the optimal SD value (Pearson's correlation $R = 0.90$, $p = 0.002$). The maximum kappa are found for smaller snow depth in the early snow season than in the late season. Similar results were obtained with the SWE, but the relationship was a slightly less significant ($R = 0.86$, $p = 0.007$).

3.2 Landsat vs. MODIS products

330 The results show that 81.5 % of the Landsat snow-covered pixels are correctly classified in MOD10A1 (Table 4). For MYD10A1 the result is similar (81.6 %), but the number of pixels that were compared is lower and the fraction of snow-covered pixels in this sample was also lower (Sect. 2.2). As a consequence, the performances are slightly better for MOD10A1 (Table 5). Figure 6 illustrates the higher dispersion of MYD10A1 with respect to Landsat

335 snow cover area. It also shows that the snow coverage tended to be underestimated by MOD10A1. The confusion matrices also indicate that MODIS has a lower snow detection than Landsat since the false negative rate is close to 18 % (Table 4). Yet, the kappa coefficients indicate a good agreement for both MODIS datasets (MOD10A1 $\kappa = 0.85$, MYD10A1 $\kappa = 0.81$, both statistically significant at the 1 % level). There is no evident dependency be-

340 tween the comparison results and the observation season (Fig. 6), which suggests that the MODIS snow detection is not significantly deteriorated by the snow properties (e.g. lower reflectance of ripe snow cover in late spring). For both MOD10A1 and MYD10A1, there is a lower agreement with Landsat when the comparison is made only over the forested areas (Table 5). However, the loss of accuracy is higher for MYD10A1. This is consistent

14

345 with the previous studies (Sect. 1). In particular, the proportion of correctly classified snow pixels drops by 9.5 % (from 81.6 to 72.1 %) in forested areas, whereas it drops by 4.1 % for MOD10A1 (from 81.5 to 77.4 %).

3.3 Gap-filling

A virtually gap-free snow cover product with a daily timestep from 1 September 2000 to 350 1 July 2013 was generated from MOD10A1 and MYD10A1. The gapfilling reduced the fraction of no-data pixels from 49 to 0.38 % (Fig. 7).The fraction of no-data decreased by a factor of about 10 to 20 % at every iteration from the previous stage, except for the spatial deduction step, which had a low effect, and the classification tree, which reduced drastically the no-data fraction by 90 %. The classification tree allowed a complete removal of the no-355 data values for all the dates for which it remained some no-data pixels after the previous steps. The 0.38 % missing values correspond to the 17 days gap in June 2001 for which the classification tree was not applicable.

We found a substantial agreement between this gapfilled product and all in situ snow depth data. The kappa coefficient ($\kappa = 0.75$, $N = 27\,684$) is a bit lower than the one obtained 360 with MOD10A1 ($\kappa = 0.79$, Table 3), but nearly equal to the one obtained with MYD10A1 ($\kappa = 0.74$).

The total snow cover area from the gapfilled product was also controlled using MOD10A2 (Fig. 8). As an example we show the hydrological year 2005–2006 to illustrate how the gapfilling made substantial changes to the initial data, and how it revealed the shape of 365 a typical snow depletion curve during the melt season. Similar results were obtained for the other years.

4 Discussion

4.1 In situ data vs. MODIS products

For the validation with in situ data, it was useful to merge the Ebro basin and Météo-France
370 databases because it enabled to expand the range in station elevation, and thus to obtain
a more robust conclusion. Kappa coefficients are within 0.74 and 0.92 depending on the
product and the variable, but the highest accuracy was obtained between MOD10A1 (Terra)
and the SWE measurements. As expected the agreement was a bit lower when considering
MYD10A1 (Aqua). The inclusion of Météo-France measurements resulted in a significant
375 decrease of the agreement (Table 3). These stations have a lower mean elevation (Table 1)
than the Ebro basin telenivometers, hence the snow cover is more discontinuous or "patchy"
in their vicinity. For example, three stations from the Météo-France dataset are located in
valley bottoms (near hydroelectricity plants), hence their spatial representativeness at the
scale of the MODIS product pixel (about 500 m) is limited.

380   In spite of these variations we could identify consistent detection thresholds in SD and
SWE (Table 4, Fig. 4). However, a clear seasonal trend was detected in the optimal SD
and SWE detection threshold (see Fig. 5 for the case of the SD). This result is interesting
because it reflects the hysteresis in the relationship between the amount of snow on the
ground and its extent, which was often observed in alpine catchments (e.g. Magand et al.,
385 2014). Small snow depths can cover large areas during the accumulation period. However,
the spatial variability of the snow depth increases over the snow season due to ablation
and redistribution processes. As a consequence, the minimum snow depth value to cover a
MODIS pixel increases over the snow season.

4.2 Landsat vs. MODIS products

390 Regarding the comparison with Landsat, we also obtained a good agreement, but a manual
screening of the comparison maps revealed that a large fraction of the misdetections was
located along the snow cover edges, in agreement with previous studies in alpine regions.

16

An example is shown in Fig. 9. The snow commission in MODIS products can be due to the effect of forest obstruction (Parajka et al., 2012) because the lower boundary of the snow cover in often situated in forested areas in the Pyrenees. In this study we could detect a deleterious effect of the forests by comparing MODIS products with Landsat over forested areas. This method assumes that the Landsat snow detection was accurate enough to be considered as a ground-truth. This assumption may not be always be valid, although the snow classification method for Landsat is well-established. Indeed we could also observe snow commission errors in our Landsat snow maps dataset along the snow cover edges. This may artificially increase the agreement with MODIS products. However, we consider that Landsat misclassifications are less frequent than MODIS.

Another possible cause for this error, which was not specifically investigated here, is the effect of the MODIS sensor view angle. This is illustrated by the image of the 18 March 2009 in Fig. 9. On this day, the Pyrenees are on the edges of both input granules from the MOD10_L2 swath product (i.e. the input data used to generate the MOD10A1), where the MODIS instrument "bowtie" effect is the most pronounced (Gómez-Landesa et al., 2004). This configuration causes a distortion of the gridded snow product MOD01A1 over the Pyrenees. The consequence is an increase of the false negative along the edges of the snow cover.

Lastly, another likely explanation is that the surface temperature screening in the snow mapping algorithm (Hall et al., 2001) is too strict so it eliminates true snow pixels in low elevation areas. The thermal threshold was discarded for the reprocessing of the collection 6 of MODIS snow products (Hall and Riggs, 2013), thus we can expect some improvements with respect to this issue at least in the next MODIS snow product release.

4.3 Gap-filling

The cloud obstruction is an important drawback of snow products generated from remote sensing instruments operating in the visible-infrared wavelengths. Here we had to interpolate an important fraction of the pixels to produce a consistent snow cover dataset (about 50%, Fig. 7). After combining Aqua and Terra snow products only 5.3% of the cloud pixels

17

were converted to snow pixels. However, this represents about the half of the total snow pixels in the final product. Hence, we further examined the cloud cover in the original product to evaluate the spatial uncertainty due to the gap-filling. We used MOD10A1 to map the probability of cloud occurrence in the study area over 2000-2013 (Fig. 10, top panel). The cloud
425 probability in the Pyrenees is more important in the north-west because the prevailing westerlies bring moist air from the North-Atlantic into the continent, whereas the south-eastern Pyrenees are more influenced by the Mediterranean climate, with a lower nebulosity. The cloud cover map also reflects the rain-shadow effect due to the orographic lifting of the air masses coming from the Atlantic by the Cantabrian mountains and the Pyrenees in the west
430 coast of the Iberian peninsula. The seasonal variability of the cloud cover also reflects the influence of both Mediterranean and oceanic climates (Fig. 10, bottom panel). The cloud cover probability decreases in summer but remains substantial throughout the year. The highest cloud probability is found in April. Unfortunately this one of the months when the snow cover monitoring is the most useful because it corresponds to the beginning or the
435 middle of the snow melt season. This is an issue especially if the MODIS products is to be used under real time conditions for river flow forecasting.

5 Application of the snow cover dataset

5.1 Spatio-temporal influences on the mean snow cover duration

The new gap-free snow cover dataset was used to compute the mean monthly snow cover
440 duration (SCD), i.e. the number of snow days in the Pyrenees. We represented here the mean SCD per elevation band to characterize the climatological influence of the elevation on the snow cover dynamics (Fig. 11). It shows that the number of snow days increases strongly from band 800–1600 m a.s.l. to band 1600–2400 m a.s.l. between November and April. This is consistent with López-Moreno and Vicente Serrano (2007), who report a 0 °C
445 isotherm around 1600–1700 m a.s.l. in the Spanish Pyrenees for the same months. Over 2400 m a.s.l. the data indicate that the snowpack covers the surface virtually all the time

18

between December and April. The melt season occurs between March and June, in agreement with e.g. Lopez-Moreno and Garcia-Ruiz (2004). There is snow on the ground at least 50% of the time above 1600 m between December and April.

⁴⁵⁰ We further analyzed the snow cover duration variability as a function of the slope's aspect for the area above 800 m a.s.l. (Fig. 12). It shows that the snow cover tends to persist longer on north-facing and east-facing slopes. This is consistent with the expected effect of the solar radiation on the snowpack energy balance. North-facing slopes receive less solar energy. West and east facing slopes are exposed to the same insolation but west-facing
⁴⁵⁵ slopes receive solar radiation in the afternoon at the hottest time of day, which explains why the snow melts faster than on the east-facing slopes. If we further normalize the SCD with respect to the mean monthly SCD (not shown here), we see more clearly that the difference between east and west facing slopes increases over the snow season (from November to June). This is consistent with the previous explanation, because the effect of the solar
⁴⁶⁰ radiation becomes more evident during the ablation season. This process is contributing to the hysteresis in the relationship between the SWE and the SCA, which was identified above (Sect. 4.1).

For this analysis we used the same elevation and aspect grid as for the gap-filling (Sect. 2.2.3). Hence, a fraction of the snow cover climatology was constructed based on
⁴⁶⁵ the same elevation and aspect data. However, this fraction is too small to significantly modify the results of this analysis (Fig.7).

5.2 Snow cover pattern in winter 2012

As above, we used the new gap-free snow cover dataset to compute the mean snow cover duration between the 1 January and 1 March for each pixel over the period 2000–2013 ex-
⁴⁷⁰ cluding 2012. The snow cover duration between the 1 January 2012 and 1 March 2012 was computed separately (Fig. 13). Both maps reveal an anomalous snow cover distribution during the winter 2012. Above-normal mean snow cover duration is observed in the northern part of the Pyrenees, contrasting with a strong snow deficit across the southern part. In situ SWE measurements in the Ebro catchment corroborate this analysis, as a large deficit was

475 also recorded in most stations (not shown here, but visible in the case of Ordiceto station Fig 3).

Given the importance of the Ebro basin for the hydroelectricity in Spain (Fig. 2), we extracted monthly energy production data in Spain from the Spanish Statistical Office database (Instituto Nacional de Estadistica, Ministerio de Industria, Energía y Turismo,
480 2013). The hydropower production dropped in early 2012 in comparison with the mean value over 1995–2012 (Fig. 14). The annual production was also lower in spite of a recovery in April–May. At the national scale the total production was higher than the 1995–2012 average (all sources of energy included), which means that the energy demand was high. Hence it is likely that the 2012 drop in hydropower production was caused by the winter 2012
485 drought in the Spanish Pyrenees, that we also observed in the snow cover data (Fig. 13). Further analysis is necessary to establish if and how the snow deficit contributed to this drop. The gross of the snowmelt generally occurs between April and July, but snow melting can be important throughout the winter in the lower elevation areas. It is also possible that hydroelectric dams managers reduced their hydropower productions in anticipation to the
490 coming deficit of snowmelt in winter.

6 Conclusions

We found an overall very good agreement between the MODIS Aqua/Terra products and two independent snow cover datasets generated from in situ (stations) and remote sensing observations (Landsat). Landsat data confirmed that the snow cover edges are prone to
495 commission (snow not detected), in particular when the sensor view angle is large. Also, the uncertainties in the final snow product increases due to the interpolation of the cloud covered pixels, in particular in the north-west Pyrenees and during the winter and spring months.

In spite of these limitations the results of this study support the conclusion that the MODIS
500 snow products provide a valuable information on snow cover at the scale of the Pyrenees range.

Using all in situ data we could determine a statistically optimal detection threshold, i.e. the snow depth or snow water equivalent value from which it is very likely that a pixel is classified as snow covered in MODIS products. We found that an acceptable SWE detection threshold is between 20 and 60 mm w.e. and a SD threshold between 100 and 120 mm for both MOD10A1 and MYD10A1. We recommend to consider these ranges of values to convert the snow depth simulated by a snowpack model into snow cover area at the MODIS resolution in the Pyrenees, e.g. for model validation or data assimilation.

The MODIS snow products should be used more carefully for hydrology because it is less accurate in the transition areas where the snowmelt is fast. But they can provide meaningful insights for climatological studies provided that the missing values are interpolated. This is particularly revealing for a transboundary mountain range like the Pyrenees where hydroclimatic observations are collected by various agencies without a joint framework or a common data depository. We used this gapfilled snow cover product to compute the climatological snow cover duration in the Pyrenees for the first time to our knowledge. This information can now be used to study the spatio-temporal dynamics of the Pyrenean snow cover since 2000. Here, we were able to reveal the asymmetrical snow patterns during the winter 2012 (Fig. 13). A strong snow cover duration anomaly is evident in the Spanish Pyrenees, reflecting a precipitation deficit which may have caused a temporary drop in the hydropower production at the national scale. In order to further use MODIS data to improve hydropower prediction, the best solution may be the assimilation of MODIS data into a hydrological model. However, an issue is the cloud cover which can reduce significantly useful data in real time conditions.

21

References

Arsenault, K. R., Houser, P. R., and De Lannoy, G. J. M.: Evaluation of the MODIS snow cover fraction product, Hydrol. Process., 28, 980–998, doi:10.1002/hyp.9636, 2014.

Ault, T., Czajkowski, K., Benko, T., Coss, J., Struble, J., Spongberg, A., Templin, M., and Gross, C.: Validation of the MODIS snow product and cloud mask using student and NWS cooperative station observations in the Lower Great Lakes Region, Remote Sens. Environ., 105, 341–353, 2006.

Baillarin, S., Gleyzes, J., Latry, C., Bouillon, A., Breton, E., Cunin, L., Vesco, C., and Delvit, J.: Validation of an automatic image orthorectification processing, IEEE T. Geosci. Remote, 2, 1398–1401, doi:10.1109/IGARSS.2004.1368680, 2004.

Baumgartner, M., Seidel, K., and Martinec, J.: Toward snowmelt runoff forecast based on multisensor remote-sensing information, IEEE T. Geosci. Remote, 746–750, 1987.

Bejarano, M. D., Marchamalo, M., de Jalón, D. G., and del Tánago, M. G.: Flow regime patterns and their controlling factors in the Ebro basin (Spain), J. Hydrol., 385, 323–335, doi:10.1016/j.jhydrol.2010.03.001, 2010.

Bossard, M., Feranec, J., and Otahel, J.: CORINE land cover technical guide – Addendum 2000, Tech. Rep. 40, European Environment Agency, Copenhagen, Denmark, 2000.

Bowley, C. J., Barnes, J. C., and Rango, A.: Satellite snow mapping and runoff prediction handbook, Tech. rep., NASA Technical Paper 1829, National Aeronautics and Space Administration, Washington, D.C., 1981.

Breiman, L., Friedman, J., Stone, C. J., and Olshen, R. A.: Classification and regression trees, CRC Press, Boca Raton, Forida, USA, 1984.

Chander, G., Markham, B. L., and Helder, D. L.: Summary of current radiometric calibration coefficients for Landsat MSS, TM, ETM+, and EO-1 ALI sensors, Remote Sens. Environ., 113, 893–903, doi:10.1016/j.rse.2009.01.007, 2009.

Cohen, J.: A coefficient of agreement for nominal scales, Educational and psychological measurement, 20, 37–46, 1960.

Dozier, J.: Spectral signature of alpine snow cover from the Landsat Thematic Mapper, Remote Sens. Environ., 28, 9–22, 1989.

Dozier, J. and Marks, D.: Snow mapping and classification from Landsat Thematic Mapper data, Ann. Glaciol, 9, 97–103, 1987.

22

Dupeyrat, A., Agosta, C., Sauquet, E., and Hendrickx, F.: Sensibilité aux variations climatiques d'un bassin à forts enjeux: le cas de la Garonne, in: Proceedings 13th IWRA World Water Congress, vol. 15, Montpellier, France, 2008.

Gómez-Landesa, E. and Rango, A.: Operational snowmelt runoff forecasting in the Spanish Pyrenees using the snowmelt runoff model, Hydrol. Process., 16, 1583–1591, 2002.

Gómez-Landesa, E., Rango, A., and Bleiweiss, M.: An algorithm to address the MODIS bowtie effect, Can. J. Remote Sens., 30, 644–650, doi:10.5589/m04-028, 2004.

Hagolle, O., Huc, M., Pascual, D., and Dedieu, G.: A multi-temporal method for cloud detection, applied to FORMOSAT-2, VENμS, LANDSAT and SENTINEL-2 images, Remote Sens. Environ., 114, 1747–1755, 2010.

Hall, D. and Riggs, G.: Accuracy assessment of the MODIS snow products, Hydrol. Process., 21, 1534–1547, 2007.

Hall, D. and Riggs, G.: MODIS snow cover products, in: Global Cryosphere Watch (GCW) Snow-Watch Workshop, Toronto, Canada, 2013.

Hall, D., Riggs, G., and Salomonson, V.: Development of methods for mapping global snow cover using moderate resolution imaging spectroradiometer data, Remote Sens. Environ., 54, 127–140, 1995.

Hall, D., Riggs, G., and Salomonson, V.: Algorithm Theoretical Basis Document (ATBD) for the MODIS snow and sea ice-mapping algorithms, Tech. rep., Goddard Space Flight Center, Greenbelt, MD, 2001.

Hall, D., Riggs, G., Salomonson, V., DiGirolamo, N., and Bayr, K.: MODIS snow-cover products, Remote Sens. Environ., 83, 181–194, 2002.

Hall, D., Riggs, G., and Salomonson, V.: MODIS/Terra Snow Cover Daily L3 Global 500 m Grid V005, National Snow and Ice Data Center, Boulder, Colorado, USA, 2006.

Hall, D., Riggs, G., and Salomonson, V.: MODIS/Aqua Snow Cover Daily L3 Global 500 m Grid V005, National Snow and Ice Data Center, Boulder, Colorado, USA, 2007.

Instituto Nacional de Estadistica, Ministerio de Industria, Energía y Turismo: Boletín Mensual de Estadística, available at: http://www.ine.es (last access: 10 June 2014), 2013.

Klein, A. and Barnett, A.: Validation of daily MODIS snow cover maps of the Upper Rio Grande River Basin for the 2000–2001 snow year, Remote Sens. Environ., 86, 162–176, 2003.

Klein, A., Hall, D., and Riggs, G.: Improving snow cover mapping in forests through the use of a canopy reflectance model, Hydrol. Process., 12, 1723–1744, 1998.

23

Lopez-Moreno, J. and Garcia-Ruiz, J.: Influence of snow accumulation and snowmelt on streamflow in the central Spanish Pyrenees, Hydrolog. Sci. J., 49, 787–802, doi:10.1623/hysj.49.5.787.55135, 2004.

López-Moreno, J. I. and Vicente Serrano, S. M.: Atmospheric circulation influence on the interannual variability of snow pack in the Spanish Pyrenees during the second half of the 20th century, Nord. Hydrol., 38, 33–44, 2007.

Magand, C., Ducharne, A., Le Moine, N., and Gascoin, S.: Introducing hysteresis in snow depletion curves to improve the water budget of a land surface model in an Alpine catchment, J. Hydrometeorol., 15, 631–649, 2014.

Maurer, E., Rhoads, J., Dubayah, R., and Lettenmaier, D.: Evaluation of the snow-covered area data product from MODIS, Hydrol. Process., 17, 59–71, 2003.

Meyer, P., Itten, K., Kellenberger, T., Sandmeier, S., and Sandmeier, R.: Radiometric corrections of topographically induced effects on Landsat TM data in an alpine environment, ISPRS J. Photogramm., 48, 17–28, 1993.

Milano, M., Ruelland, D., Dezetter, A., Fabre, J., Ardoin-Bardin, S., and Servat, E.: Modeling the current and future capacity of water resources to meet water demands in the Ebro basin, J. Hydrol., 500, 114–126, 2013.

Ministerio de Agricultura, Alimentación y Medio Ambiente: Inventario de Presas y Embalses, available at: http://www.magrama.gob.es/es/agua/temas/seguridad-de-presas-y-embalses/ inventario-presas-y-embalses/ (last access: 10 June 2014), 2011.

Paquet, E. and Laval, M.-T.: Retour d'expérience et perspectives d'exploitation des Nivomètres à Rayonnement Cosmique d'EDF/Operation feedback and prospects of EDF Cosmic-Ray Snow Sensors, La Houille Blanche, 2, 113–119, 2006.

Parajka, J. and Blöschl, G.: Validation of MODIS snow cover images over Austria, Hydrol. Earth Syst. Sci., 10, 679–689, doi:10.5194/hess-10-679-2006, 2006.

Parajka, J. and Blöschl, G.: Spatio-temporal combination of MODIS images–potential for snow cover mapping, Water Resour. Res, 44, W03406, doi:10.1029/2007WR006204, 2008.

Parajka, J., Holko, L., Kostka, Z., and Blöschl, G.: MODIS snow cover mapping accuracy in a small mountain catchment – comparison between open and forest sites, Hydrol. Earth Syst. Sci., 16, 2365–2377, doi:10.5194/hess-16-2365-2012, 2012.

Parra, M. A., Campos, G. C., and Alonso-Muñoyerro, J. M.: El programa ERHIN y la gestión de embalses en áreas con alta precipitación nival, Ingeniería civil, 89–96, 2006.

Rango, A.: II. Snow hydrology processes and remote sensing, Hydrol. Process., 7, 121–138, 1993.

Rittger, K., Painter, T. H., and Dozier, J.: Assessment of methods for mapping snow cover from MODIS, Adv. Water Resour., 51, 367–380, 2013.

Rived, R. A., González Alvarez, M. A., and Ballarín, G. L.: Evidence of employment niches in tourism: an intra-regional approach, Tourism Econ., 19, 707–717, doi:10.5367/te.2013.0221, 2013.

Salomonson, V. and Appel, I.: Estimating fractional snow cover from MODIS using the normalized difference snow index, Remote Sens. Environ., 89, 351–360, 2004.

San Ambrosio, I., Buisan, S., Rodriguez, J., and Vada, J. A.: Climatological comparison of 2011–2012 and 2012–2013 winters focused on the huge contrast in different nivological parameters in Pyrenees range (Spain), in: International Snow Science Workshop 2013, Grenoble, France, 2013.

Simic, A., Fernandes, R., Brown, R., Romanov, P., and Park, W.: Validation of VEGETATION, MODIS, and GOES+ SSM/I snow-cover products over Canada based on surface snow depth observations, Hydrol. Process., 18, 1089–1104, 2004.

Sirguey, P., Mathieu, R., Arnaud, Y., Khan, M., and Chanussot, J.: Improving MODIS Spatial Resolution for Snow Mapping Using Wavelet Fusion and ARSIS Concept, IEEE Geosci. Remote S., 5, 78–82, doi:10.1109/LGRS.2007.908884, 2008.

Sociedad Española de Presas y Embalses: Inventario de Presas Españolas, available at: http://www.seprem.es/presases.php (last access: 10 June 2014), 2008.

Table 1. Description of the in situ snow data used in this study. Stations 1 to 11 are telenivometers from the ERHIN program for which daily data of snow depth and snow water equivalent were available. Stations 12 to 19 are Météo-France stations for which daily data of snow depth only were available. Longitude and latitude are given in decimal degrees (WGS84) and elevation in m a.s.l.

ID	Name	Longitude	Latitude	Elevation	Period
1	Quimboa	−0.76	42.87	1810	Oct 2008–Jan 2013
2	Izas	−0.43	42.75	2080	Oct 2008–Aug 2012
3	Roya	−0.45	42.79	1971	Oct 2008–Feb 2013
4	Bachimana	−0.22	42.79	2220	Oct 2008–Jan 2013
5	Lapazosa	−0.08	42.71	2140	Oct 2008–Jun 2012
6	Ordiceto	0.28	42.67	2380	Oct 2008–Feb 2013
7	Renclusa	0.65	42.67	2180	Oct 2008–Feb 2013
8	Salenques	0.70	42.61	2600	Oct 2008–Jul 2013
9	Eriste	0.45	42.63	2350	Oct 2008–Jan 2013
10	Airoto	1.03	42.71	2380	Oct 2008–Feb 2013
11	Aixeus	1.37	42.61	2400	Oct 2008–Jun 2013
12	Aulus-Les-Bains	1.33	42.80	733	Jan 2000–Dec 2010
13	Mont-Dolmes	1.75	42.85	1500	Jan 2000–Dec 2010
14	Port-Daula	1.12	42.77	2140	Jan 2000–Dec 2010
15	Maupas	0.55	42.72	2430	Oct 2000–Dec 2010
16	Bagneres-de-Luchon	0.60	42.80	620	Jan 2003–Dec 2010
17	St-Paul-Doueil	0.55	42.83	1115	Dec 2004–Dec 2010
18	Eget	0.27	42.78	1016	Jan 2000–Dec 2010
19	St-Lary-Soul	0.32	42.82	827	Jan 2000–Dec 2010

Table 2. Confusion matrices between the MODIS snow products and in situ data. The numbers correspond to percentage with respect to the number of in situ measurements. The comparison was performed both for snow water equivalent ("SWE") and snow depth ("SD") measurements. The detection thresholds were set to $SWE_0 = 40$ mm w.e. for SWE and $SD_0 = 150$ mm for SD. These thresholds yielded the best kappa coefficients.

	MOD10A1		MYD10A1	
	no snow	snow	no snow	snow
	Telenivometers			
$SWE < SWE_0$	97	2.7	97	2.8
$SWE > SWE_0$	2.2	98	2.6	97
$SD < SD_0$	96	4.2	95	4.6
$SD > SD_0$	4.1	96	4.2	96
	All stations			
$SD < SD_0$	92	8.1	89	11
$SD > SD_0$	13	87	15	85

Table 3. Statiscal measures of the comparison between MODIS product and in situ data, computed from the results presented in Table 2 (N: sample size, A: overall accuracy, κ: kappa coefficient).

	MOD10A1			MYD10A1		
	Telenivometers		All stations	Telenivometers		All stations
	SD	SWE	SD	SD	SWE	SD
N (10^3)	7.4	7.9	11.4	6.7	6.7	9.1
A	0.96	0.98	0.89	0.97	0.96	0.87
κ	0.92	0.95	0.79	0.94	0.91	0.74

Table 4. Confusion matrix obtained from the comparison of Landsat snow maps with Aqua/Terra MODIS snow maps. The numbers correspond to percentage with respect to Landsat data. The results are given for all the study area ("all"), and the area covered by forests only ("forest").

		MOD10A1			
		No snow		Snow	
		all	forest	all	forest
Landsat	No snow	99.0	98.1	1.00	1.93
	Snow	18.5	22.6	81.5	77.4
		MYD10A1			
		No snow		Snow	
		all	forest	all	forest
Landsat	No snow	98.2	96.9	1.85	3.12
	Snow	18.4	27.9	81.6	72.1

Table 5. Statistical measures of the comparison between MODIS products and Landsat, computed from the results presented in Table 4 (N: sample size, A: overall accuracy, κ: kappa coefficient). The results for the forested areas are indicated in parentheses.

	MOD10A1	MYD10A1
N (10^6)	14.7 (5.41)	11.2 (4.05)
A	0.97 (0.96)	0.96 (0.95)
κ	0.85 (0.77)	0.81 (0.67)
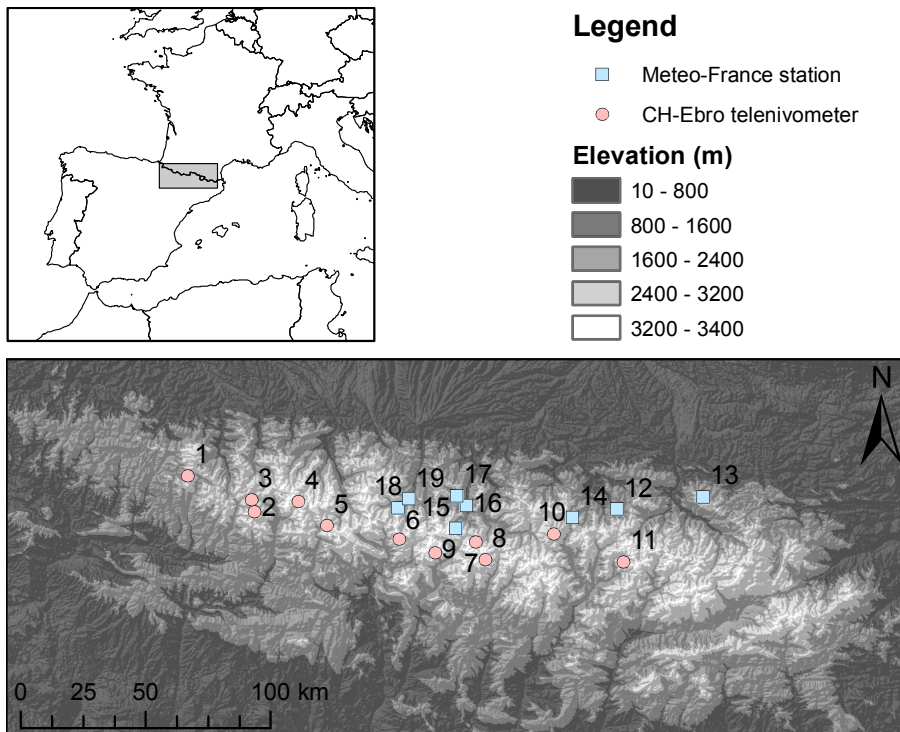
Figure 1. Shaded relief map of the study area and location of the snow monitoring stations used in this study (map projection Lambert-93). The rectangle is the area of interest used for remote sensing data (corner coordinates: upper left $x = 320$ km, $y = 6250$ km, lower right $x = 680$ km, $y = 6100$ km).
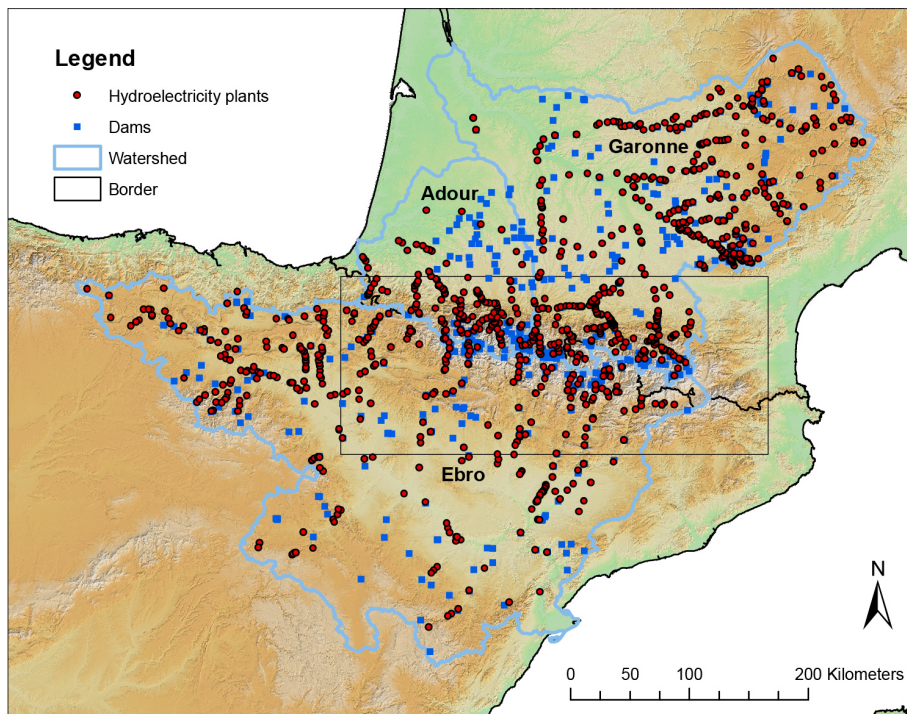
Figure 2. Hydraulic infrastructures in the Adour, Garonne and Ebro rivers basins.
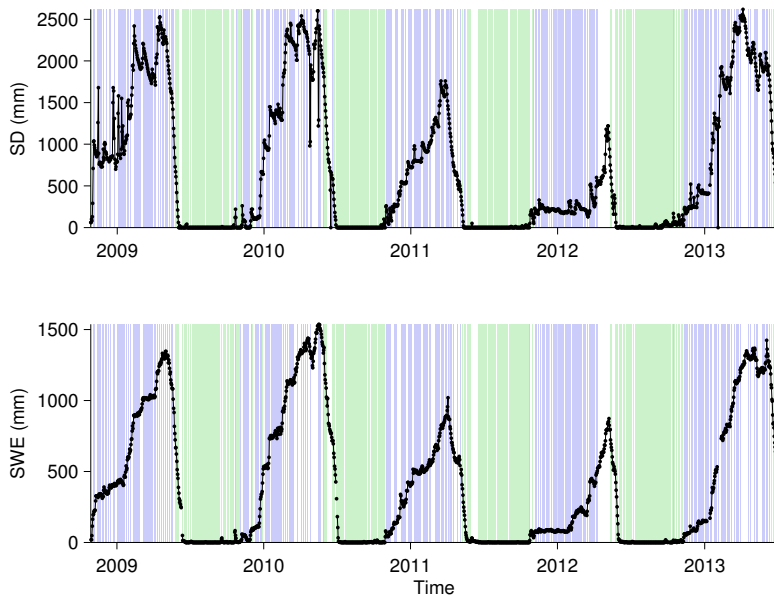
Figure 3. Timeseries of in situ data and MODIS data at Ordiceto station. The black dots are the daily snow depth (SD) and snow water equivalent (SWE) measurements. The color bars in the background indicate the snow presence (blue), absence (green) and no data (white) from MOD10A1.

33
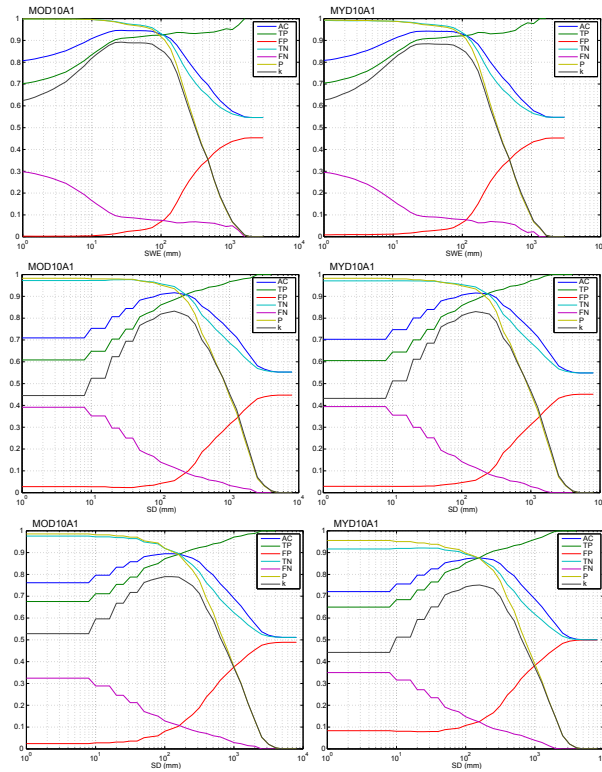
Figure 4. Comparison of MODIS products with in situ data. Top row: reference data are the SWE measurements from the telenivometers, middle row: SD measurements from the telenivometers, bottom row: SD data from all stations. Each graph shows the variation of the statistical agreement between both datasets with the snow detection threshold: AC: overall accuracy, TP: true positive, FP: false positive, TN: true negative, FP: false positive, P: precision, k: kappa coefficient.
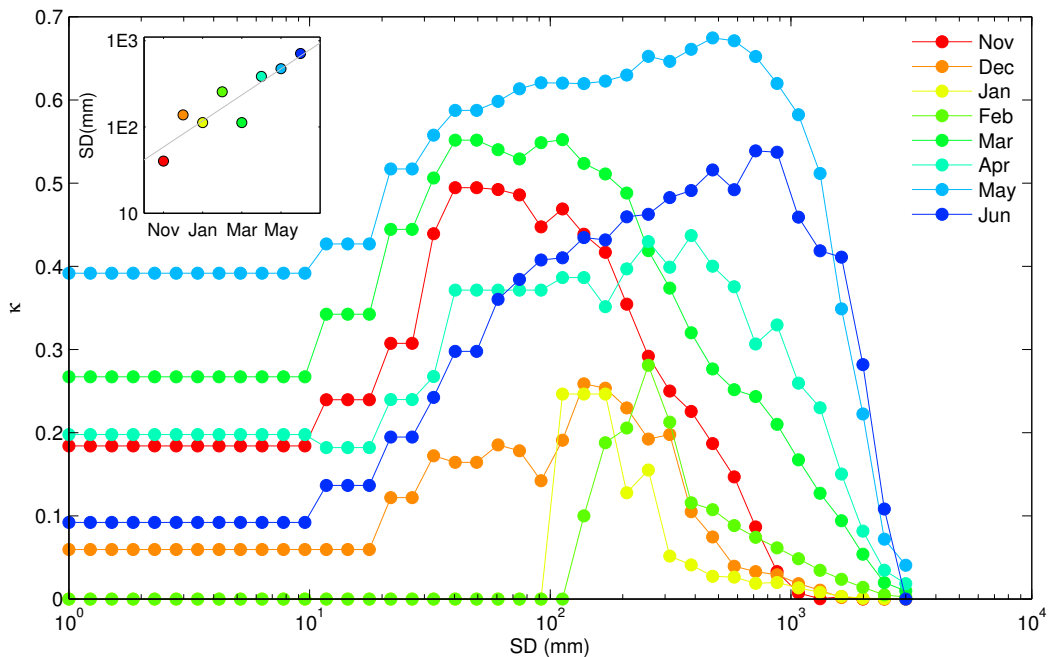
Figure 5. Evolution of the kappa coefficient with the value of the snow depth detection threshold for each month of the snow season. Here only the telenivometers data and the MOD10A1 product were considered. The snow depth value giving the maximum kappa was extracted for each month and plotted against the month (inset). The linear fit was calculated with log-transformed values of the SD (Pearson's correlation $R = 0.90$, $p = 0.002$)
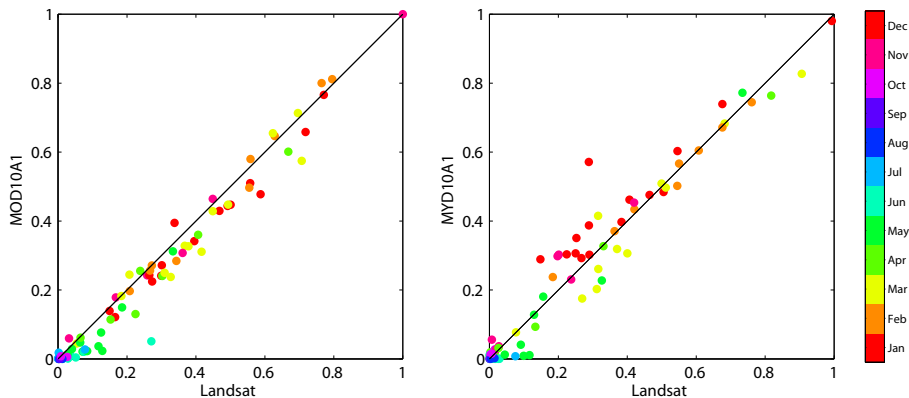
Figure 6. Snow coverage calculated from Landsat and MODIS snow products (Terra MOD10A1, Aqua MYD10A1) for 157 dates (139 dates for MYD10A1) distributed between 2002 and 2010 over the Pyrenees. The color indicates the month of the year. The snow coverage is defined as the fraction of the cloud-free area which is covered by snow in the study area (Fig. 1). For each date, the cloud-free area is defined as the intersection of the cloud-free areas in Landsat and MODIS products.

36
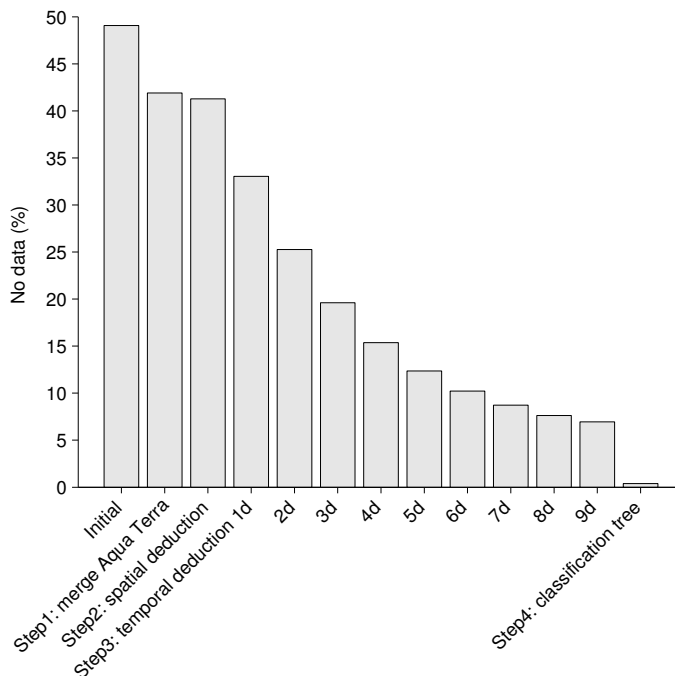
Figure 7. Evolution of the number of pixels classified as "no-data" (e.g. clouds) during the gapfilling procedure.
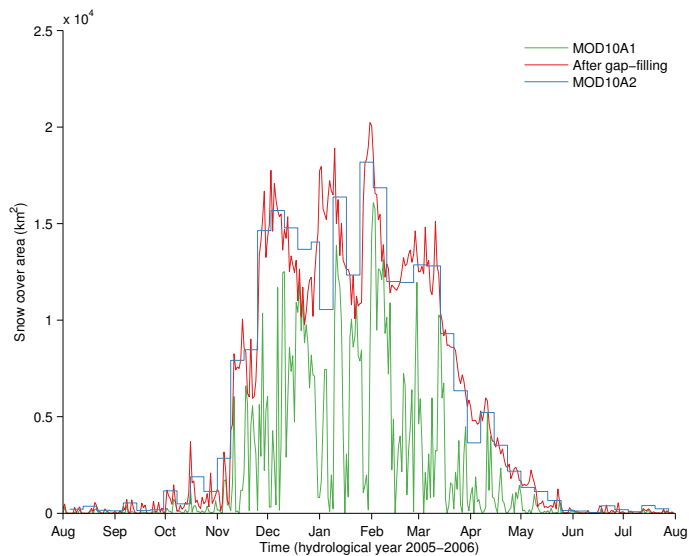
Figure 8. Snow cover area evolution in the Pyrenees over the hydrological year 2005–2006 for three products: MOD10A1, the gap-filled product from MOD10A1 and MYD10A1 (this study) and MOD10A2 (8 day maximum snow extent).
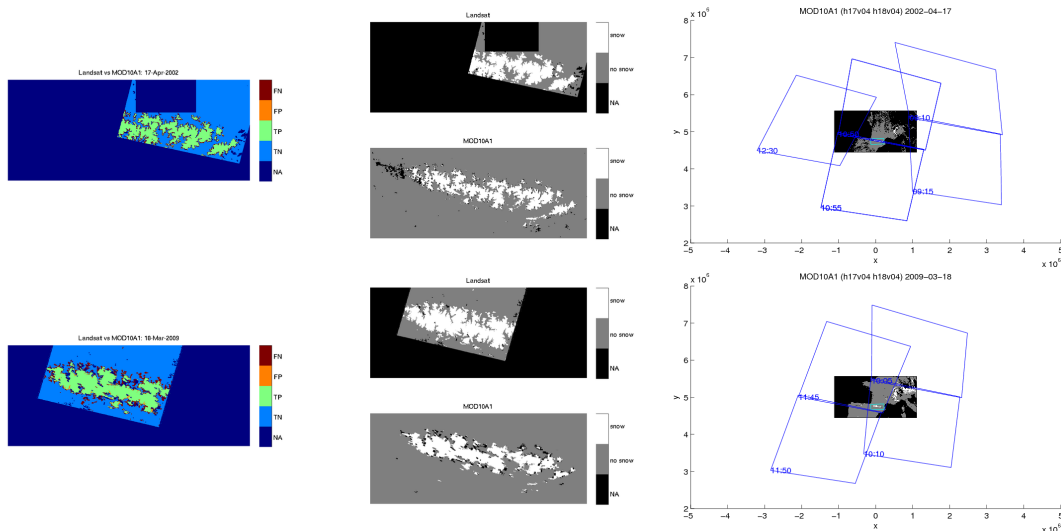
Figure 9. Comparison between MOD10A1 and Landsat for two dates. Left column: MOD10A1 vs. Landsat classification (TP: true positive, FP: false positive, TN: true negative, FP: false positive). MOD10A1 false negative are mainly located along the snow cover edges. Middle column: Landsat and MOD10A1 classifications used for the comparison. Right column: location of the input swath granules (MOD10_L2 product) used to generate the MOD10A1 tiles (sinusoidal map projection). The MOD10A1 snow mask is distorted on 18 March 2009 because it was constructed from the border areas of two input granules where the bowtie effect is most pronounced.
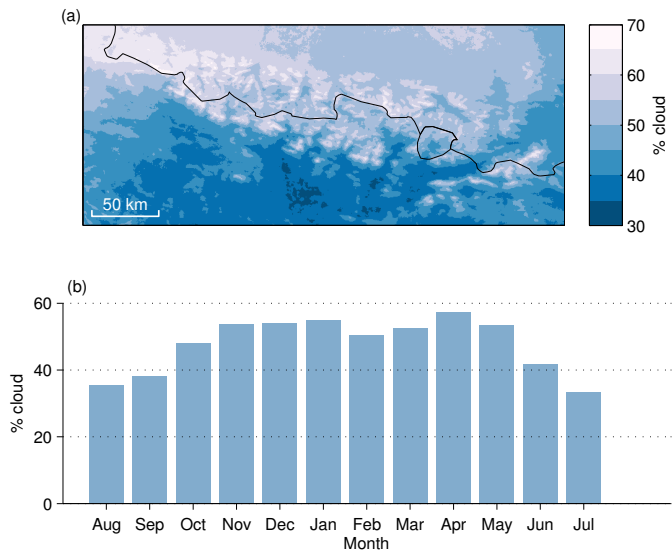
Figure 10. (a) Fraction of cloud covered pixels in MOD10A1 over 2000–2013 (b) Mean monthly cloud coverage from MOD10A1 in the study area.
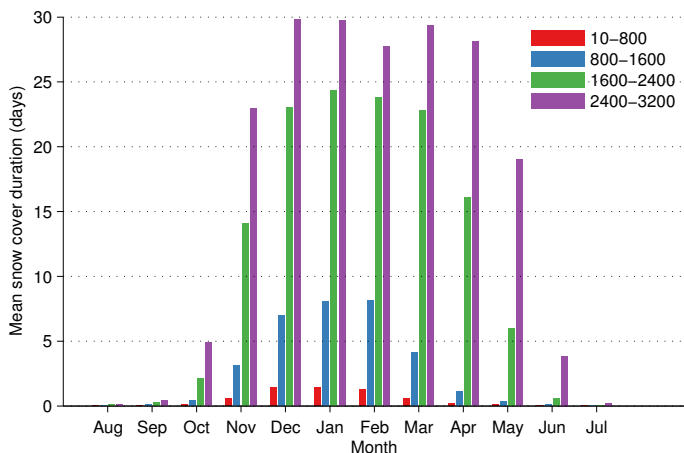
40

Figure 11. Mean snow cover duration in the Pyrenees over 2000–2013 for different elevation bands. The snow cover duration is the number of days with snow in our gapfilled product. It was computed with the same elevation bands as Fig. 1, except for 3200–3400 m a.s.l. (only 4 pixels at the MODIS resolution). Otherwise the fractional areas of each elevation band in the study domain are: 53 % (10–800), 31 % (800–1600), 13 % (1600–2400), 2.5 % (2400–3200).
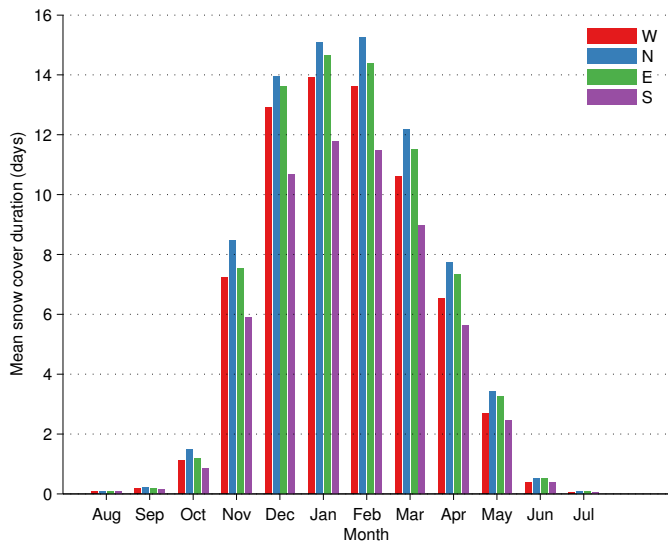
Figure 12. Mean snow cover duration in the Pyrenees over 2000–2013 for the four main aspect classes (W:west-facing slopes, N:north-facing slopes, E:east-facing slopes, S:south-facing slopes). The snow cover duration was computed only for the area above 800 m a.s.l..
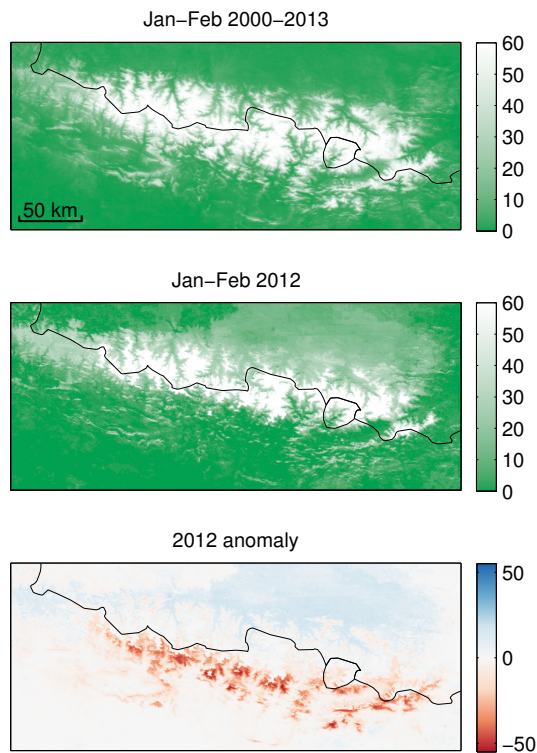
Figure 13. Illustration of the anomalous snow patterns in the Pyrenees during the winter 2012. Top panel: mean snow cover duration (days) in January and February, Middle panel: snow cover duration in January and February 2012. Bottom panel: snow cover duration anomaly.
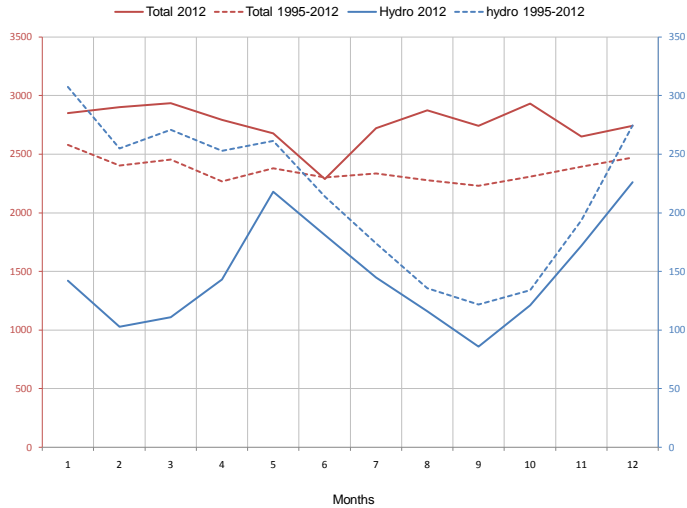
Figure 14. Monthly energy production in Spain (units: kTep). The right y axis is for hydropower, the left y axis is for the total energy production.